IOPscience iopscience.iop.org

Home Search Collections Journals About Contact us My IOPscience

Monte Carlo simulation of terahertz generation in nitrides

This article has been downloaded from IOPscience. Please scroll down to see the full text article.

2001 J. Phys.: Condens. Matter 13 7159

(http://iopscience.iop.org/0953-8984/13/32/318)

View the table of contents for this issue, or go to the journal homepage for more

Download details:
IP Address: 171.66.16.226
The article was downloaded on 16/05/2010 at 14:06

Please note that terms and conditions apply.

INSTITUTE OF PHYSICS PUBLISHING JOURNAL OF PHYSICS: CONDENSED MATTER

J. Phys.: Condens. Matter **13** (2001) 7159–7168 PII: S0953-8984(01)24822-X

Monte Carlo simulation of terahertz generation in nitrides

E Starikov[1], P Shiktorov[1], V Gružinskis[1], L Reggiani[2], L Varani[3], J C Vaissière[3] and Jian H Zhao[4]

[1] Semiconductor Physics Institute, A Goštauto 11, 2600 Vilnius, Lithuania
[2] Dipartimento di Ingegneria dell' Innovazione, Istituto Nazionale di Fisica della Materia, Università di Lecce, Via Arnesano s/n, 73100 Lecce, Italy
[3] Centre d'Electronique et de Micro-Optoélectronique de Montpellier (CNRS UMR 5507), Université Montpellier II, 34095 Montpellier Cédex 5, France
[4] SiCLAB, Department of Electrical and Computer Engineering and CAIP Center, Rutgers University, Piscataway, NJ 08855, USA

Received 14 May 2001
Published 26 July 2001
Online at stacks.iop.org/JPhysCM/13/7159

Abstract
The conditions for microwave power generation under the quasi-periodic motion of carriers caused by the combined action of carrier acceleration in a constant electric field and optical phonon emission at low temperatures are analysed by means of Monte Carlo simulations of both small- and large-signal responses in bulk nitrides such as GaN and InN. It is shown that, as a consequence of the high value of the optical phonon energy and the strong electron–phonon interaction, a dynamic negative differential mobility caused by transit-time resonance occurs over a wide frequency range which covers practically the whole submillimetre range and persists in the THz frequency range up to liquid nitrogen temperature. The efficiency of the amplification and generation is found to depend nonmonotonically on: (i) the static and microwave electric field amplitudes, (ii) the generation frequency, and (iii) the carrier concentration. Accordingly, for each generation frequency there exists an optimal range of parameter values. Under optimal conditions we predict a generation efficiency of about 1–2% in the 0.5–1.5 THz frequency range.

1. Introduction

The recent observation of microwave generation in n-InP at low lattice temperatures [1] has confirmed the possibility of the so-called optical phonon transit-time resonance (OPTTR) maser widely discussed during the last few decades [2–6]. The generation is associated with the periodic motion of a carrier inside the optical phonon sphere in momentum space when a constant electric field E_0 is applied to a bulk material at low lattice temperatures (typically

 © 2001 IOP Publishing Ltd Printed in the UK

well below 77 K). Because of the acceleration by the electric field, a carrier moves quasi-ballistically up to the optical phonon energy $\hbar\omega_0$, quickly emits an optical phonon, and returns back inside the optical phonon sphere, from where the next cycle of acceleration is started. The characteristic average transit time (or period of oscillations) is given by $\tau_E = p_0/eE_0$ where p_0 is the radius of the optical phonon (OP) sphere. Due to the oscillatory character of this motion, a dynamic negative differential mobility (DNDM) will appear at frequencies near the inverse of the transit time and its harmonics [2–4]. The resulting instability corresponds to amplification and generation of the transverse electromagnetic waves propagating in a homogeneous active medium and is not related to any space-charge effects. The higher the coherence of successive free flights (and, hence, the DNDM maximum value), the weaker the scattering intensity inside the OP sphere (the so-called passive region) and the carrier penetration into the active region where optical phonon emission is possible. In standard III–V semiconductors, such as GaAs and InP, the frequency range of generation was predicted to be restricted to the sub-THz range up to frequency values of about 300–400 GHz [5]. The upper limit of generation frequency is mainly due to carrier penetration into the active region occurring at increasing values of the applied electric field. Therefore, the stronger the carrier–phonon interaction, the weaker the penetration, and, hence, the higher the upper frequency limit for appearance of the generation. At the present time the strongest carrier–phonon interaction is thought to be achieved in wide-gap semiconductors such as nitrides (InN, GaN, etc) and SiC. For this reason, in these materials one can expect a considerable increase of the maximum generation frequency up to the super-THz range and a general improvement of the conditions for DNDM. The aim of the present work is to confirm this expectation by carrying out a theoretical investigation of the generation band and associated features for an OPTTR maser based on bulk InN and GaN.

2. Theoretical background

The most important characteristics of any generator are the spectrum and the power of the generated radiation. The behaviour of both these quantities can be described in terms of the so-called dynamic amplification coefficient (the dynamic gain) defined as [7]

$$\alpha_\omega(U) = -\frac{\sqrt{\epsilon}}{c}\frac{P_\omega(U)}{U} \tag{1}$$

where U is the single-mode radiation energy density inside the volume of the semiconductor under test, $P_\omega(U)$ the generated (or absorbed) radiation power density, ϵ the relative static dielectric constant of the material, c the light velocity in vacuum, f the frequency, $\omega = 2\pi f$ the cyclic frequency. The radiation energy density U can be written as

$$U = \frac{1}{T_\omega}\int_0^{T_\omega} \epsilon_0\epsilon|E(t)|^2\,\mathrm{d}t \tag{2}$$

where $E(t) = \mathrm{Re}[E_\omega \exp(\mathrm{i}\omega t)]$ is the microwave (MW) electric field, $T_\omega = 2\pi/\omega = 1/f$ the period of the MW electric field, and ϵ_0 the vacuum permittivity. In turn, the power density generated by the active medium is given by

$$P_\omega = \frac{1}{T_\omega}\int_0^{T_\omega} en\langle v(t)\rangle E(t)\,\mathrm{d}t \tag{3}$$

where e is the electron charge, n the carrier concentration, and $\langle v(t)\rangle$ the average drift velocity during a period of the MW field. According to its definition, P_ω takes negative values in the region of generation, so the dynamic gain is positive in this case. Substitution of equations (2) and (3) into equation (1) yields the amplification coefficient in its conventional form:

$$\alpha_\omega = -\mathrm{Re}[\mu_\omega]n\frac{e}{c\epsilon_0\sqrt{\epsilon}} \tag{4}$$

where $\mathrm{Re}[\mu_\omega] = 2P_\omega/enE_\omega^2$ is the real part of the carrier MW mobility which takes negative values under generation conditions. Notice that equations (1) and (4) are general and hold true for both linear and nonlinear regimes of the MW radiation interaction with the medium.

Under linear operation conditions, when $U \to 0$, α_ω is independent of U and:

(i) it determines the frequency region of amplification,
(ii) it is an estimate for the threshold value for the net losses at which the generation is still possible,
(iii) it allows one to choose the optimal concentration n for a given sample, etc.

Furthermore, $\mathrm{Re}[\mu_\omega]$ coincides with the differential mobility spectrum which for given conditions can be calculated at once by using velocity averaging over pre- and post-scattering ensembles during a Monte Carlo (MC) simulation of the single-carrier history as described in [5, 6].

Under nonlinear operation conditions, α_ω depends on U and knowledge of it forms the basis for the analysis of the stable generation of an active medium placed inside an external resonant system [8]. Indeed, the stability of the generation process implies that all radiation losses are exactly compensated by the radiation amplification due to DNDM inside the system. Therefore, under stable generation of the single-mode radiation, the dynamic gain is equal to the coefficient of the net loss in the resonant system, $\alpha_L = \Gamma + \Lambda$. It includes both the outside power extraction, as described by the coefficient coupling the active medium with the external free space, Γ, and all the parasitic losses in the resonant system, as described by the coefficient of internal losses, Λ. Therefore, one can finally represent the power generated inside the resonator as a function of α_L by $P_{gen}(\alpha_L) = -P_\omega(\alpha_\omega)$. The simulation of the nonlinear response allows us to obtain the function $P_\omega(U)$ and to calculate $\alpha_\omega(U)$ in accordance with equation (1). To calculate $P_\omega(U)$ and $\alpha_\omega(U)$ in accordance with equations (1)–(3) the average MW drift velocity $\langle v(t)\rangle$ is directly calculated by using the MC simulation of the velocity response to a MW electric field $E(t)$ superimposed on a constant value E_0. Then, by eliminating U from $P_\omega(U)$ and $\alpha_\omega(U)$—that is, by expressing P_ω as a function of α_ω—one obtains the dependence of the output power extracted from the OPTTR maser upon the generalized parameters of the resonator:

$$P_{out} = P_{gen}(\alpha_L)\frac{\Gamma}{\Gamma + \Lambda}. \tag{5}$$

3. Numerical results

As follows from equations (3) and (4), both the gain and the generated power should increase with the increase of the carrier concentration controlled by the doping level. However, the increase of the carrier concentration in turn decreases the value of $-\mathrm{Re}[\mu_\omega]$, and, hence, of both α_ω and P_ω. The competition of these two opposite tendencies implies the existence of an optimum range of doping level for each generation frequency where the gain and the generated power are maxima. Moreover, on one hand, the DNDM must be absent at low values of the applied constant field E_0, since the impurity scattering destroys entirely any ballistic motion. On the other hand, the DNDM must disappear at sufficiently high E_0 due to the large penetration of carriers into the active region which destroys the coherence of successive free flights. Therefore, the DNDM depends nonmonotonically on frequency and applied field. To take into account properly all these effects and the competition of opposite tendencies, numerical calculations were performed by means of MC simulations. Below, we shall present the most important optical characteristics for an InN and GaN OPTTR THz maser obtained

by MC simulations in accordance with the theoretical framework presented above. Electron scatterings by polar optical phonons, deformation acoustic phonons and ionized impurities are accounted for. The parameters of the band models and scattering mechanisms are taken from [9–11].

3.1. Small-signal operation

Figure 1 reports the frequency and field behaviour of the real part of the differential mobility Re μ calculated for zinc-blende GaN at $T = 10$ K and $n = 10^{16}$ cm^{-3}. The OPTTR manifests itself in a sequence of minima of Re μ corresponding to the first and higher harmonics of the resonant frequency $\nu_E = 1/\tau_E$ (see curve 2). However, the broadening of the minima increases significantly for higher harmonics so a DNDM is achieved usually at the first minimum only. Let us refer to the frequency where the DNDM takes the maximum value for a given E_0 as the optimal amplification frequency, f_{opt}. Curves 1 to 5 show the variation of the first minimum with the increase of the electric field. In the low-field region (see curves 1 and 2), the appearance and rapid growth of the amplification is connected with the electron runaway from the low-energy region dominated by impurity scattering, which causes the otherwise quasi-ballistic motion to deteriorate. With a further increase of E_0 the maximum value of the gain decreases approximately as $1/E_0$ (see curves 2 to 5). Finally, at $E_0 \approx 10$ kV cm^{-1} the gain disappears due to a significant penetration of carriers into the active region, which destroys the coherence of successive free flights.

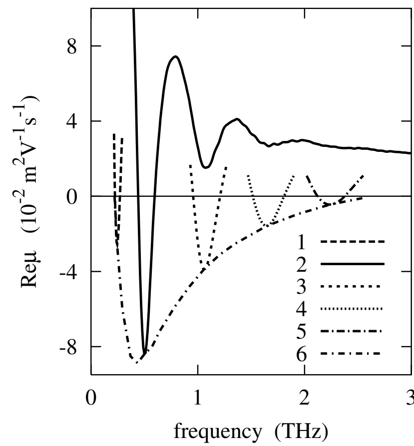

Figure 1. General behaviour of the differential mobility spectrum (curve 2), variation of the resonance region at different electric fields (curves 1 to 5 for $E = 1, 2, 4, 6, 8$ kV cm^{-1}), and maximum value of the DNDM (curve 6) as functions of frequency.

Figure 2 reports the maximum gain and the corresponding static field, α_ω and E_0, respectively, as functions of the optimal amplification frequency f_{opt} for zinc-blende and wurtzite GaN samples with $n = 10^{16}$ cm^{-3} at $T_0 = 10$ and 80 K. The difference in OPTTR characteristics between the zinc-blende and wurtzite modifications of GaN is mainly related to the difference in the effective mass (0.15 and 0.2, respectively) and usually does not exceed 20%. As follows from figure 2, the MW amplification caused by the OPTTR covers practically the whole submillimetre range ($f = 0.3$–3 THz) for the same GaN sample with a carrier concentration of about 10^{16} cm^{-3} and persists in the THz frequency range at least up to liquid nitrogen temperature. Similar results are obtained for InN.

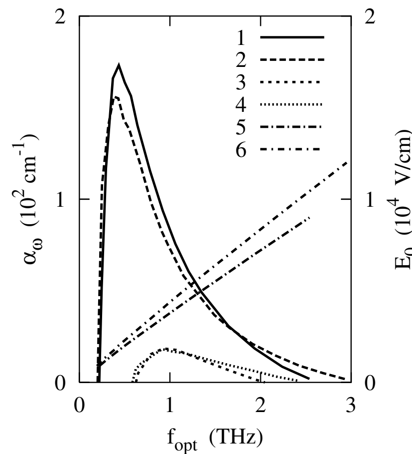

Figure 2. Maximum values of the small-signal gain (curves 1 to 4) and corresponding values of the applied static electric field (curves 5, 6) as functions of the optimal amplification frequency f_{opt} for zinc-blende (curves 1, 3, 5) and wurtzite (curves 2, 4, 6) GaN samples with $n = 10^{16}$ cm^{-3} at $T_0 = 10$ (curves 1, 2, 5, 6) and 80 K (curves 3, 4).

Figure 3 presents the maximum DNDM and the amplification coefficient for different concentration levels of InN samples (curves 1 to 4 for $n = 1, 3, 10, 30 \times 10^{15}$ cm^{-3} in the lower and upper parts of figure 3, respectively) as functions of the optimal amplification frequency. Curve 5 in the upper part refers to the static E_0 corresponding to a given value of f_{opt}. As usual, the maximum values of the DNDM are achieved for low carrier concentrations

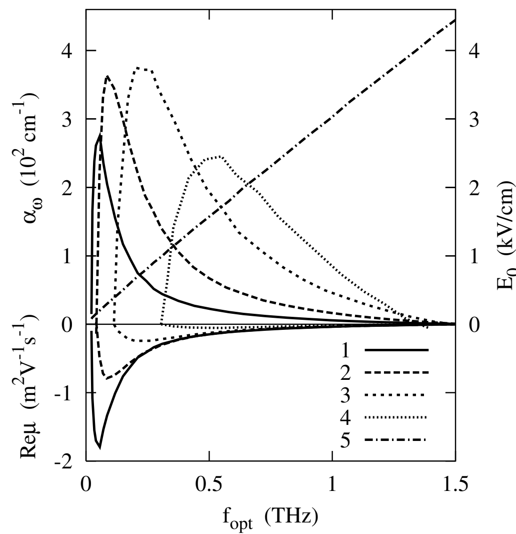

Figure 3. Maximum values of the DNDM and amplification coefficient (lower and upper parts, respectively, and left-hand scale of the figure) calculated for different concentration levels of InN samples (curves 1 to 4 for $n = 1, 3, 10, 30 \times 10^{15}$ cm^{-3}), and the static field E_0 corresponding to a given value of f_{opt} (curve 5 and right-hand scale of the figure) as functions of the optimal amplification frequency.

in the low-field region (and, accordingly, in the low-frequency region of the amplification) just after the electron runaway from the low-energy impurity scattering has taken place. With the increase of n the onset for DNDM is shifted to higher electric fields, so the DNDM maximum in the low-field region first decreases (curve 2) and finally disappears completely (curves 3 and 4). At the same time, in the high-field region the corresponding high-frequency values of the DNDM remain practically unchanged. Of course, with a further increase of the carrier concentration up to $n \approx$ (5–6) $\times 10^{16}$ cm^{-3}, the DNDM in this region also disappears. In other words, a concentration increase is practically always accompanied by a DNDM decrease. By contrast, within an intermediate concentration level, the amplification coefficient usually increases with n especially in the high-frequency region, thus leading to different values of the optimum concentration in different spectral ranges. As follows from figure 3, for the case of InN the optimum values of n are of about (0.5–1) $\times 10^{16}$ cm^{-3} for the MW amplification at $f \leqslant 0.5$ THz and of about (2–3) $\times 10^{16}$ cm^{-3} in the higher-frequency range.

In the case of GaN the ranges of optimum concentration levels are similar to those for InN. This is illustrated by figure 4, which presents the maximum small-signal gain at five fixed frequencies $f = 0.25, 0.5, 1, 1.5, 2$ THz (and, respectively, at five different values of the static field $E_0 = 1.2, 2.25, 4.3, 6.35, 8.35$ kV cm^{-1}) as functions of the electron concentration in wurtzite GaN at $T_0 = 10$ K.

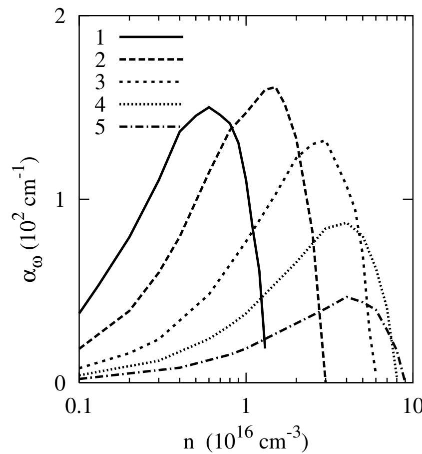

Figure 4. Small-signal gain calculated as a function of electron concentration in wurtzite GaN at $T_0 = 10$ K for $f = 0.25, 0.5, 1, 1.5, 2$ THz (curves 1 to 5).

The increase of the lattice temperature always leads to a decrease of both the DNDM and the amplification coefficient due to the increase of the scattering intensity in the passive region. This is illustrated in figure 5 which presents the variation of α_ω with temperature T in InN at four fixed frequencies $f = 0.25$ THz for $n = 10^{16}$ cm^{-3} (curve 1) and $f = 0.5, 0.75, 1$ THz for $n = 3 \times 10^{16}$ cm^{-3} (curves 2 to 4). The wide temperature range of amplification so found offers favourable conditions for obtaining generation experimentally at both liquid helium and liquid nitrogen temperatures.

3.2. Large-signal operation

To achieve generation it is necessary to insert the active medium into a resonator system which must satisfy some conditions. In the presence of DNDM, an external resonant system will lead to the onset and growth of MW oscillations accompanied with an increase of the amplitude of

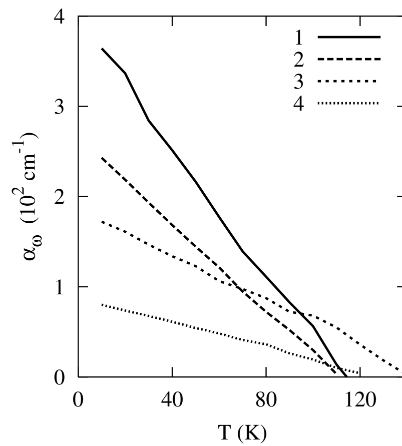

Figure 5. The temperature dependence of α_ω at frequencies $f = 0.25$ THz calculated for InN with $n = 10^{16}$ cm^{-3} (curve 1) and $f = 0.5, 0.75, 1$ THz for $n = 3 \times 10^{16}$ cm^{-3} (curves 2 to 4).

E_ω inside the sample. Therefore, the nonlinear analysis of generation is performed through a direct modelling of the velocity response under a large-signal operation at a given frequency by the MC method. As an example, figure 6 presents the generated power and the dynamical gain calculated in accordance with equations (3) and (1), respectively, as functions of the MW electric field amplitude E_ω at frequency $f = 0.75$ THz for InN with carrier concentration $n = 3 \times 10^{16}$ cm^{-3} at $T = 10$ K. The static field value $E_0 = 2.4$ kV cm^{-1} corresponds to the maximum amplification coefficient for these conditions (see figure 3). With the increase of E_ω the generated power $P_{gen} = -P_\omega$ first increases, reaches a maximum, and finally goes to zero since a high MW field destroys the OPTTR. Correspondingly, the dynamical gain α_ω starts from its small-signal value and monotonically goes to zero. By representing P_{gen} as a function of α_ω one then can evaluate the optimum conditions for MW power generation at each given frequency.

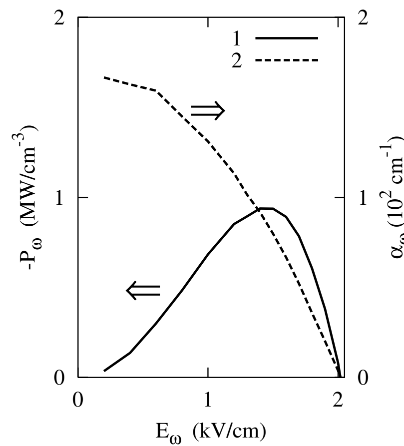

Figure 6. Generated power and dynamical gain calculated for InN as functions of the MW electric field amplitude E_ω. The calculations were performed with the following parameters: $f = 0.75$ THz, $E_0 = 2.4$ kV cm^{-1}, $n = 3 \times 10^{16}$ cm^{-3}, $T = 10$ K.

Figures 7 and 8 summarize the results of the large-signal calculations for wurtzite GaN and InN, respectively. Figure 7(a) reports the absolute value of the power density generated in wurtzite GaN as a function of the coefficient of net losses in the resonant system, α_L. Different curves refer to different frequencies $f = 0.25, 0.5, 1, 1.5$, and 2 THz and, respectively, to different static electric fields $E_0 = 1.2, 2.25, 4.3, 6.35$, and 8.35 kV cm^{-1} which correspond to the maximum value of the small-signal gain at a given frequency (see figure 2). For each curve the carrier concentration is chosen to provide the maximum values of P_ω. The corresponding efficiency of generation is presented in figure 7(b). Let us recall that for a stable generation the dynamical gain must exactly compensate all the losses in the resonant system due to power extraction outside the resonator, parasitic, etc, i.e. $\alpha_\omega = \alpha_L$. Thus, if at a given frequency α_L exceeds the small-signal gain, α_ω^0, given by the linear theory (see figure 4), then generation is absent. Therefore, with the decrease of α_L, at each given frequency the generation starts from the value of the small-signal gain. With a subsequent decrease of α_L, the power increases and reaches a maximum value at the optimum amplitude of the MW field. As follows from figure 7(a), this optimum value is achieved when $\alpha_L \simeq 0.5\alpha_\omega^0$. Here, a generation efficiency of about 1–2% is achieved (see figure 7(b)). With a further decrease of α_L, the amplitude of the MW field increases so much that it would destroy the transit-time resonance. For this reason, the generated power decreases, to finally vanish at $\alpha_L = 0$. Similar results obtained for the MW power generation in InN are presented in figure 8. Here, one can see that even in the sub-THz region ($f = 0.5$–1 THz) GaN can provide values of the generated power and efficiency which are greater than those for InN. Moreover, in bulk GaN the generation can be achieved also at frequencies above 1 THz which is in practice difficult to achieve in the case of InN.

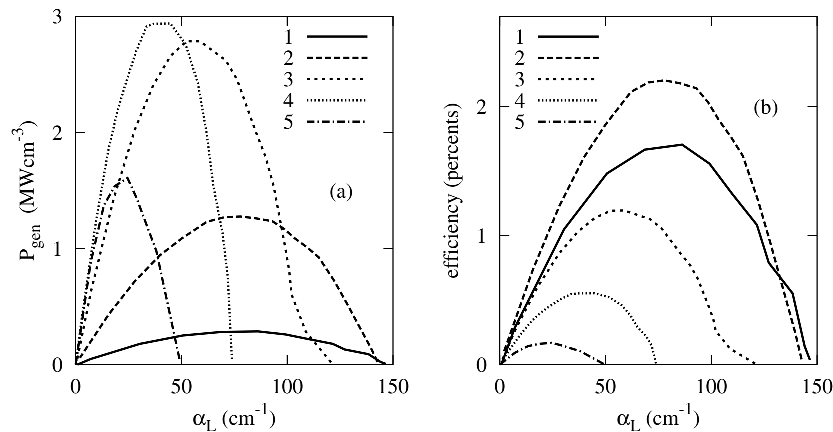

Figure 7. (a) Generated power and (b) efficiency of generation at the fundamental frequencies of $f = 0.25, 0.5, 1, 1.5$, and 2 THz (curves 1 to 5) as functions of the coefficient of total losses inside the resonator, α_L, calculated for wurtzite GaN at $T_0 = 10$ K. Curves 1 to 5 correspond to the optimal values of n and E_0, given, respectively, by $n = 0.6, 1, 2, 3, 4 \times 10^{16}$ cm^{-3} and $E_0 = 1.2, 2.25, 4.3, 6.35, 8.35$ kV cm^{-1}.

4. Conclusions

The results of both linear and nonlinear studies of the optical phonon transit-time resonance in InN and GaN performed by MC simulation show that wide-gap nitrides are promising materials for power generation in the THz frequency range. By comparison with the situation

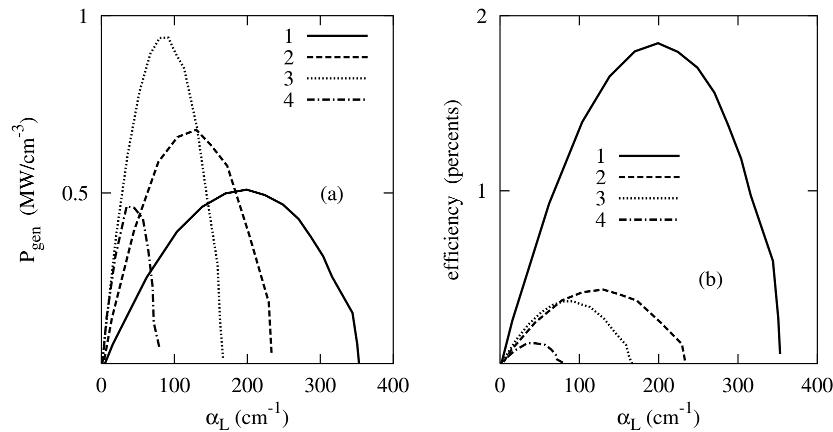

Figure 8. (a) Generated power and (b) efficiency of generation at the fundamental frequencies of $f = 0.25, 0.5, 0.75$, and 1 THz (curves 1 to 4) as functions of the coefficient of total losses inside the resonator, α_L, calculated for wurtzite InN at $T_0 = 10$ K. Curves 1 to 4 correspond to the optimal values of n and E_0, given, respectively, by $n = 1, 3, 3, 3 \times 10^{16}$ cm^{-3} and $E_0 = 0.85, 1.65, 2.4, 3.14$ kV cm^{-1}.

for standard III–V semiconductors, the high values of both the polar optical phonon energy and the electron–phonon interaction strength allow one:

(i) to considerably increase the maximum values of the constant applied field at which DNDM is still possible, and, hence, to expand the generation spectrum up to the THz frequency range,
(ii) to increase the optimum concentration level up to ionized impurity concentrations of $n = (2–4) \times 10^{16}$ cm^{-3}, which results in sufficiently high values of the amplification coefficient and generated power,
(iii) to expand the working temperature range up to liquid nitrogen temperature at least, which considerably simplifies the experimental implementation of the effect.

By comparing the characteristics of the MW power amplification and generation provided by InN and GaN, one can conclude that in the sub-THz region InN offers generally the highest values of the gain, but the lowest values of the generated power and efficiency. The frequency range of generation is larger in the case of GaN, where sufficiently high values of P_{gen} and efficiency can be achieved even in the super-THz region at frequencies of about 1–2 THz.

Acknowledgments

The authors wish to acknowledge the support of the NATO collaborative-linkage grant PST.CLG.976340, the French–Lithuanian bilateral cooperation No 5380 of the French CNRS, the MADESS II project of the Italian Consiglio Nazionale delle Ricerche (CNR), and the CAIP Center of Rutgers University.

References

[1] Vorob'ev L, Danilov S, Kochegarov Yu, Tulupenko V and Firsov D 1999 *4th Russian Conf. on the Physics of Semiconductors (Novosibirsk)* abstracts, p 42
[2] Andronov A and Kozlov V 1973 *Pis. Zh. Eksp. Teor. Fiz.* **17** 124

[3] Gulyaev Yu and Chusov I 1978 *Fiz. Tverd. Tela* **20** 2637
[4] Matulis A and Chenis A 1979 *Sov. Phys.–JETP* **50** 572
[5] Pozhela Yu, Starikov E and Shiktorov P 1992 *Semicond. Sci. Technol.* **7** B386
[6] Starikov E, Shiktorov P, Gružinskis V, Reggiani L, Varani L, Vaissière J C and Zhao J H 2001 *J. Appl. Phys.* **89** 1161
[7] Starikov E V and Shiktorov P N 1986 *Sov. Phys.–Semicond.* **20** 677
[8] Yariv A 1975 *Quantum Electronics* 2nd edn (New York: Wiley)
[9] Foutz B, Eastman L, Bhapkar U and Shur M 1997 *Appl. Phys. Lett.* **70** 2849
[10] Albrecht J, Wang R, Ruden P, Farahmand M and Brennan K 1998 *J. Appl. Phys.* **83** 4777
[11] O'Leary S, Foutz B, Shur M, Bhapkar U and Eastman L 1998 *J. Appl. Phys.* **83** 826